Theoretical Eye Model with Aspherics*

W. LOTMAR
Swiss Office of Weights and Measures, CH 3084 Wabern, Switzerland
(Received 2 April 1971)

A model for the human eye is proposed, similar to Gullstrand's well-known 4-radius model, however with the front surface of the cornea and the back surface of the crystalline lens taken to be rotationally symmetric aspherics. Whereas for the cornea a polynomial is used based on experimental data of Bonnet, a second-order parabola was tentatively adopted for the back surface of the lens. This model results in slight spherical undercorrection, in agreement with experimental findings. On the other hand, the sine condition is not well satisfied, probably due to neglect of the shell structure of the lens. By ray tracing, astigmatism and coma as well as the meridional and sagittal focal lengths were computed up to a visual angle of 90°. Calculations were also made for the same model preceded by a plano-concave contact lens (Goldmann 3-mirror contact glass), showing that this combination results in considerably reduced astigmatism.
INDEX HEADINGS: Aberrations; Image formation; Ray tracing.

In preventive treatment of human retinal detachment by photocoagulation, the aberrations of the dioptric apparatus prevent exact focusing in the far periphery of the fundus oculi, because they increase rapidly with visual angle; in particular, they impair both observation and coagulation efficiency. We have shown that these difficulties can be overcome to a large extent by use of a plano-concave contact lens (mirror contact glass of Goldmann.)[1,2] Hence it was desirable to gain some insight into the optical properties of the system, eye plus contact glass, as compared to those of the unaided eye.

In perimetry of the peripheral parts of the eye, so-called refractional scotomas are known to occur.[3,4] These are areas of reduced contrast sensitivity due not to a disturbance of the neuro-visual system but to abnormal blur of the target image. Such blur may be caused by local bulging of the retina or variation of the focal length of the optical media. Because correct diagnosis of sensitivity depressions is of course highly important, knowledge about the aberrations of the normal eye could be expected to be useful.

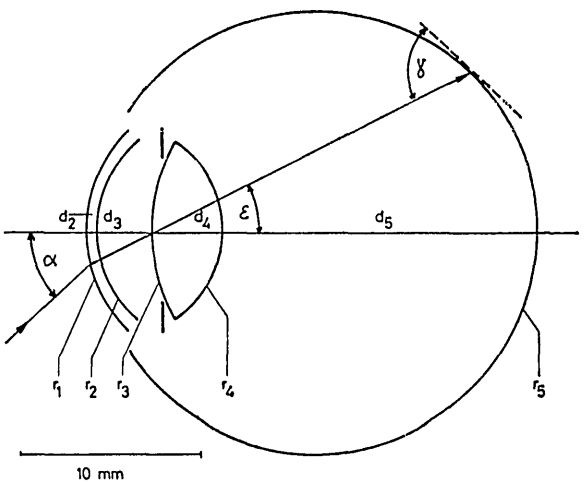

FIG. 1. Theoretical eye model of Gullstrand–Le Grand. α, visual angle; ϵ, internal angle; γ, angle of acceptance.

Another problem that arises in biomicroscopy of the eye is the determination of the absolute dimensions of objects and structures in the periphery of the retina. Little is known about the dependence of the effective focal length of the eye on visual angle.

Ferree and Rand[5] and recently Rempt *et al.*[6] have shown that the astigmatic difference (Sturm's interval) in the periphery of emmetropic human eyes varies considerably within the population. For a visual angle of 60°, values between 2 and 10 diopters have been reported, the higher figures being preponderant. From theoretical considerations, such a wide spread in a system as simple as that of the eye appeared rather strange, because for its radii, spacings, and refractive indices no large variations are known. Experimentally, Sturm's interval is measured in diopters, whereas values computed from a model are in millimeters. To convert the latter to the former both meridional and sagittal focal lengths of the eye must be known as a function of visual angle.

Finally, it is well known that the use of an indentor considerably improves the observation of the far periphery and the *pars plana*. However, quantitative predictions of the possible improvement were not available before for lack of optical data.[7]

Ray tracing through a theoretical eye model, based on recent data about the cornea profile and the correction on axis, should yield some pertinent information, although this should serve as a first approximation only. Lee *et al.*[8] reported recently on ray

TABLE I. The eye model of Gullstrand–Le Grand.

Radius (mm)	Spacing (mm)	Refractive index n_d	Medium
$r_1 = +7.8$		1.0	air
$r_2 = +6.5$	$d_2 = 0.55$	1.3771	cornea
$r_3 = +10.2$	$d_3 = 3.05$	1.3374	aqueous
$r_4 = -6.0$	$d_4 = 4.0$	1.420	lens
$r_5 = -12.3$	$d_5 = 16.60$	1.336	vitreous
	$f = 22.29$ mm		

tracing through the eye preceded by a meniscus contact lens, but gave no quantitative results.

EYE MODEL

As in previous theoretical eye models, we assume the optical system of the eye to consist of four centered refracting surfaces of rotational symmetry. The retina, too, is approximated by a spherical surface centered on the same axis. Our first model is that of Listing–Gullstrand, slightly improved by newer data of Le Grand (Fig. 1).[9] The data are given in Table I. The spacing between the lens and the retina, d_5, equals the intersection length of the preretinal media for an object at infinity, in order to make the model eye paraxially emmetropic.

Like Gullstrand, we assume a homogeneous lens, neglecting the shell structure for lack of exact data; this provides us with a relatively simple system for the calculations.

A detailed analysis of the shell structure of the rabbit-eye lens was made by Nakao *et al.*[10]; by ray tracing, they showed that this structure has a pronounced effect on the optical correction of the lens. Similar data for the human lens would also be desirable for derivation of a better model, but the calculations would have to be much more involved.

As is well known, the Gullstrand model results in strong spherical undercorrection on axis. This is quite at variance with recent experimental findings. These show that the normal unaccommodated eye, broadly speaking, is spherically corrected.[11–13] Undercorrection is of course expected for such a system when the refracting surfaces are spherical.

As a first refinement of the Gullstrand model, we assume an aspherical, rotationally symmetric shape for the front surface of the cornea, with the same radius of curvature at the vertex. When this shape closely approximates the actual geometry, we expect calculated corrections that approach reality better than the Gullstrand model not only on-axis but also for off-axis visual angles. Our results seem to confirm this.

THE FORM OF THE CORNEA

To obtain the true shape of the cornea, several experimental methods have been used. One of the most precise appears to be stereophotogrammetry as applied by Bonnet.[14,15] He was able to fit his measurements to the analytical expression (see Fig. 2),

$$\log_{10}\beta = k\alpha + b, \qquad (1)$$

where α is the angle between the normal to the profile curve and the optical axis, β is the angle between this normal and the radius of the osculating circle drawn from the intersection point of the normal with this circle, and k and b are constants for the individual cornea, which may vary somewhat for different meridians of a given cornea.

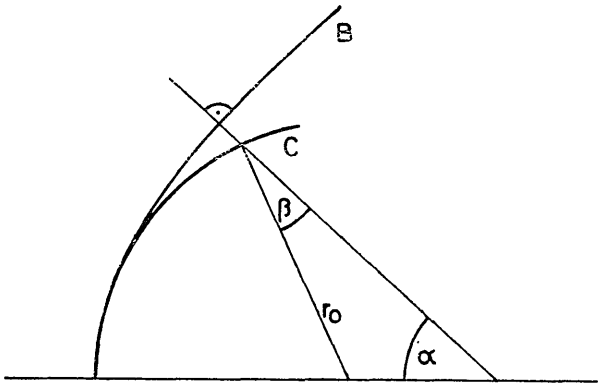

FIG. 2. Definition of angles in Eq. (1). B, profile curve of Bonnet; C, osculating circle.

For 200 emmetropic eyes measured with a special keratometer, Bonnet found that these constants are distributed around average values of +3 and −3, respectively, with a near-gaussian distribution and a mean deviation of about 1.1. With these average values,

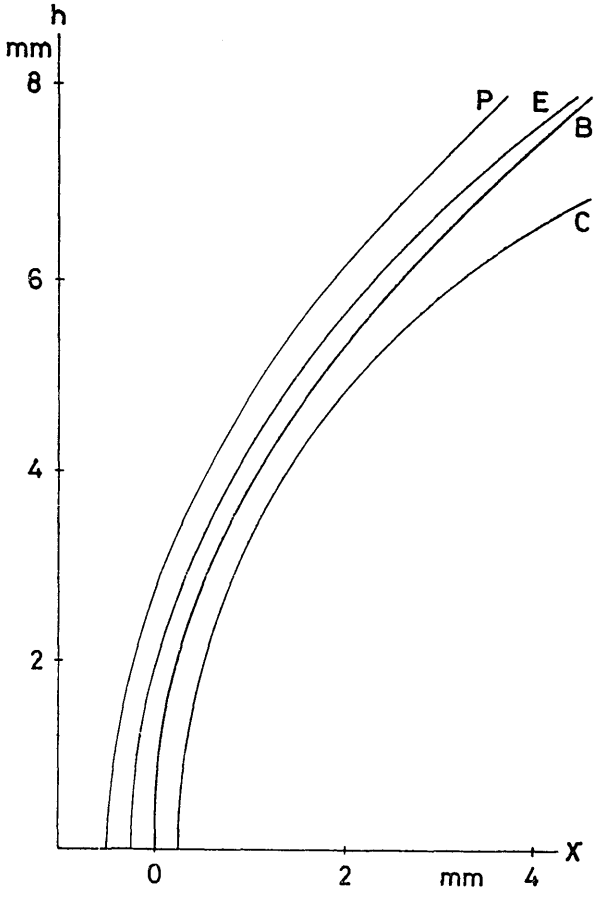

FIG. 3. B, Bonnet's profile curve for the cornea according to Eq. (3); C, osculating circle; E, ellipse; P, parabola.

the formula for the corneal profile Eq. (1) becomes

$$\log_{10}\beta = 3(\alpha - 1), \tag{2}$$

with α and β in radians.

For ray tracing by computer, we have approximated this relation by a power series,

$$x = \frac{h^2}{2r_o}\left[1 + \frac{5}{28}\left(\frac{h}{r_o}\right)^2 - \frac{1}{12}\left(\frac{h}{r_o}\right)^4\right], \tag{3}$$

x being the coordinate along the optical axis, h the distance from this axis, and r_o the radius of curvature at $h=0$ (osculating circle). The curve described by Eq. (3) is denoted by B in Fig. 3. α and β are calculated from Eq. (3),

$$\tan\alpha = 1/x' = dh/dx \tag{4}$$

$$\sin\beta = (x + hx' - r_o)\sin\alpha / r_o. \tag{5}$$

Values of β obtained from Eq. (5) agree with those from Eq. (2) to better than 0.003 rad up to $h=7$ mm and deviate by 0.03 rad for $h=8$ mm.

For comparison, three other profile curves are shown in Fig. 3, all having the same radius of curvature for $h=0$. Le Grand's value of 7.8 mm was taken for this radius (r_o) in all cases. The curves are (a) a circle, C, (b) the ellipse that intersects the polynomial Eq. (3) at

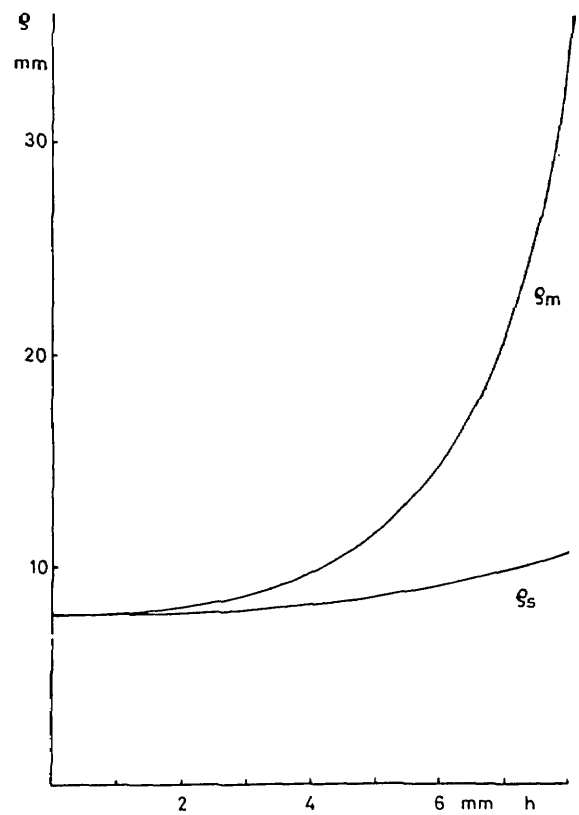

FIG. 4. Meridional and sagittal radii of curvature ρ_m and ρ_s, respectively, of body of revolution corresponding to polynomial of Eq. (3).

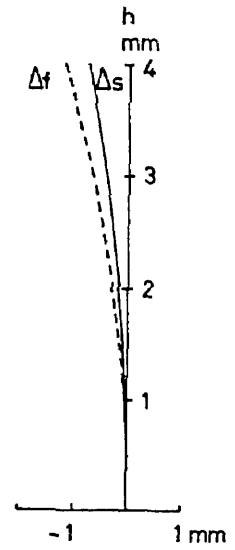

FIG. 5. Spherical aberration of eye model according to data of Table I with aspherics. Δs, aberration of intersection length; Δf, aberration of focal length.

$h=7$, E, and (c) a second-order parabola, P. In Fig. 4, the principal radii of curvature of the surface of revolution described by Eq. (3) are shown as a function of h (note $r_o=7.8$). The meridional radius of curvature ρ_m can be approximated by

$$\rho_m \cong r_o[1 + 8(h/10)^4] \tag{6}$$

and the sagittal radius by

$$\rho_s \cong r_o(1 + 1.66\times 10^{-3} h^{2.6}). \tag{7}$$

Ray tracing through this model showed an over-all spherical undercorrection of about one half that of the Gullstrand model, whereas the spherical aberration of the corneal front surface alone was practically fully corrected. This was taken to mean that in reality the balance of undercorrection is compensated by the lens. The simplest modification of the model that would re-

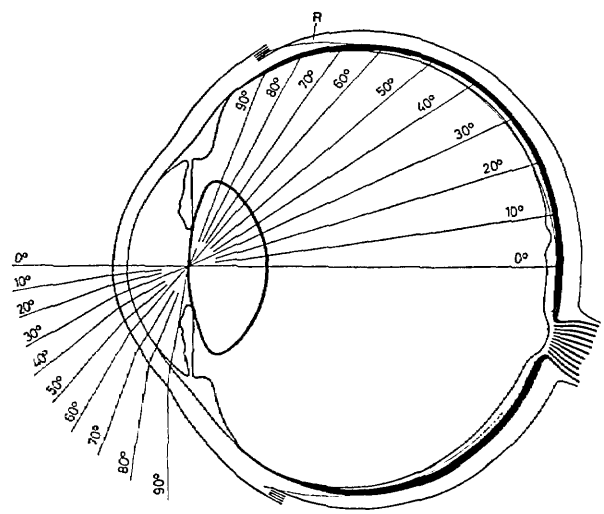

FIG. 6. Le Grand's eye model. Course of principal rays. R, schematized retina (r_5 of Table I).

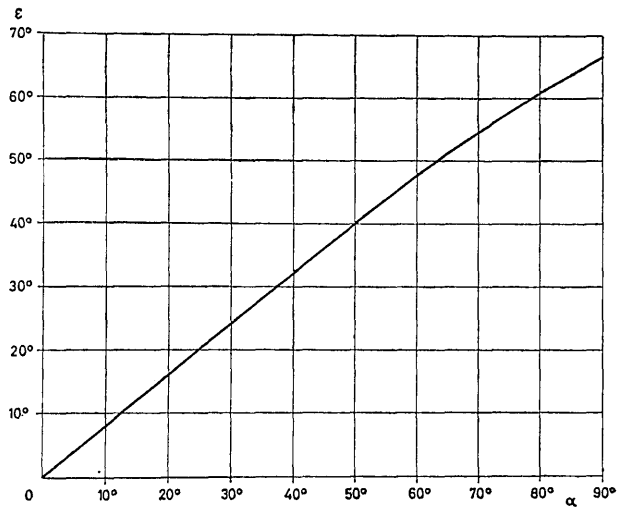

FIG. 7. Plot of internal angle ϵ vs visual angle α.

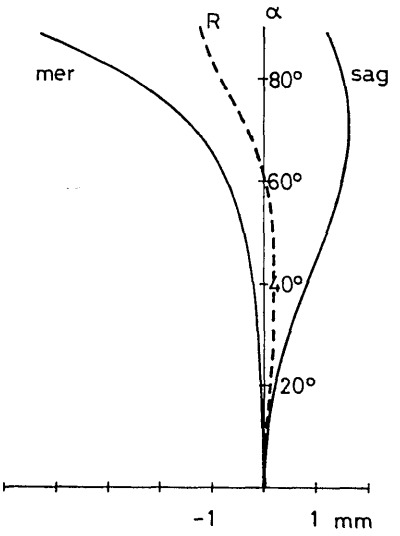

FIG. 9. Astigmatism of eye model of Table I with aspherics. Ordinate axis represents reference image sphere r_5. R, position of retina according to Le Grand.

sult in the same effect was the introduction of a second aspherical surface. We adopted the form of a parabola for the back surface of the lens, again retaining curvature at the vertex as given in Table I. For this surface, the exact shape is less critical than for the cornea because the difference of the refractive indices is much smaller (0.08 as compared to 0.38). It is well known that the backsurface of the lens is not spherical, but no exact data are available at present.

The axial spherical aberration of this model is shown in Fig. 5. It is small and of the order found experimentally. Therefore, this set of data was used for more extensive ray tracing.

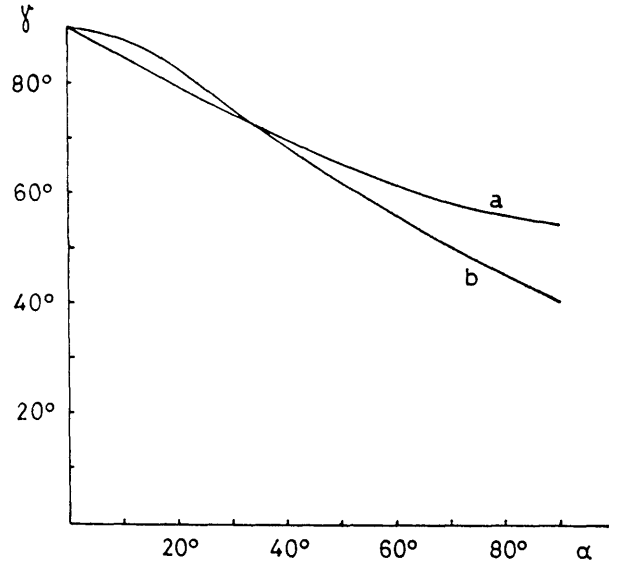

FIG. 8. Angle of acceptance γ vs visual angle α. (a) for model retina, (b) for Le Grand's cross section (Fig. 6).

RESULTS OF RAY TRACING

We traced parallel bundles of rays in the meridional plane for visual angle[16] α up to 90° in steps of 10°, assuming an apparent diameter of 8 mm of the eye pupil. The latter was taken to be a diaphragm of zero thickness adjacent to the front surface of the lens. Principal rays were made to intersect that surface at its intersection with the optical axis.

Figure 6 shows the cross section of the eye according to Le Grand, with traces of the principal rays. In Fig. 7 the internal angle ϵ of principal rays is plotted vs visual angle, where ϵ is the angle between the ray in the vitreous and the optical axis (see Fig. 1). The angle of acceptance γ; i.e., the angle between the principal ray and the retina, is plotted vs visual angle in Fig. 8, (a) for the model retina of radius 12.3 mm, and (b) as determined graphically for Le Grand's cross section (Fig. 6), however, averaging over the temporal and nasal side. Astigmatism is plotted in Fig. 9 with the sagittal focus calculated from known formulas. As is customary in ophthalmology, the distances are measured along the

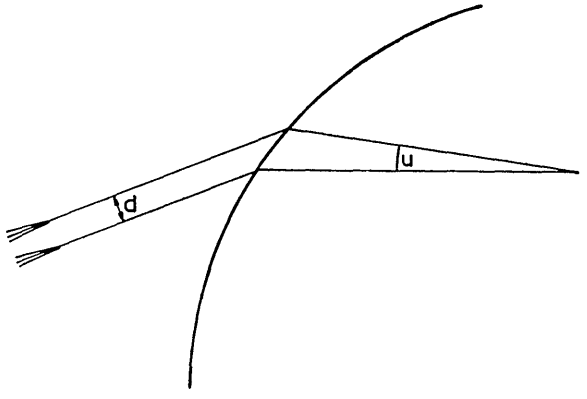

FIG. 10. Definition of focal length for oblique incidence of a parallel meridional bundle, $f_m = d/u$.

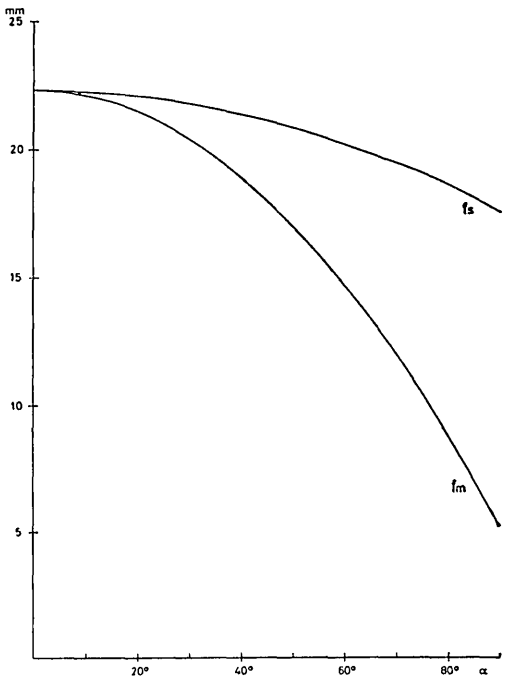

FIG. 11. Meridional and sagittal focal lengths, f_m and f_s, respectively, vs visual angle for eye model of Table I with aspherics.

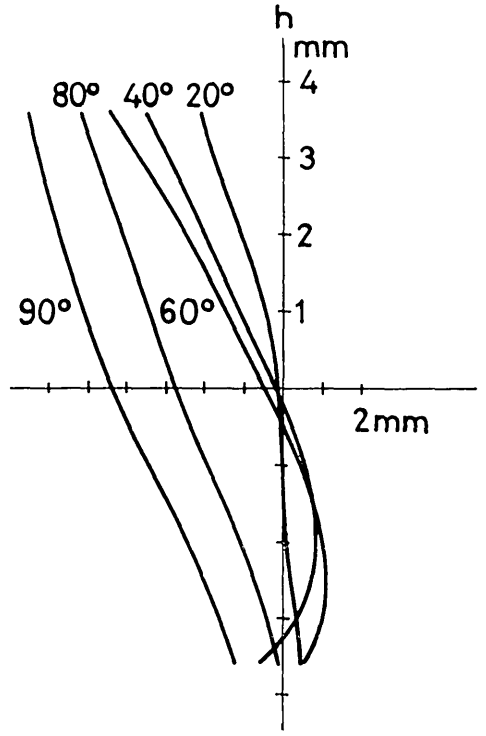

FIG. 13. Longitudinal comatic aberration of eye model with aspherics. Reference image sphere is r_5 of Table I. Plotted curves are projections of true curves on h axis along the principal rays of the corresponding bundles.

principal rays, not by projection on the axis as in lens design. Moreover, we have to keep in mind that the medium is the vitreous humor (not air). The foci are plotted by reference to a spherical retina. The true position of the retina is also indicated in the figure.

For an evaluation of image size and energy density on the retina we have to know not only the positions of the meridional and sagittal focus on the principal rays, but also the corresponding focal lengths. We can obtain these quantities by applying first-order optical imagery to the principal rays, taking the finite angles of incidence at the refracting surfaces into account. The meridional focal length f_m is defined, as for paraxial rays, by the ratio of a (infinitesimally small) distance d between the

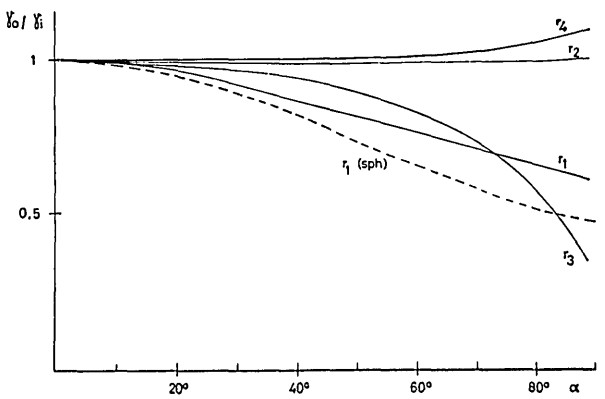

FIG. 12. Convergence ratio of individual refracting surfaces of eye model with aspherics. r_1 (sph), curve if the front surface of cornea is spherical.

incident principal ray and another parallel ray in the meridional plane, to the angle u that these rays form in the image space[17] (see Fig. 10). An analogous definition applies to the sagittal focal length f_s. Values of f_m and f_s for the model of Table I with aspherics are shown in Fig. 11 as a function of visual angle.

The meridional focal length f_m decreases considerably towards the periphery. To account for this result it is

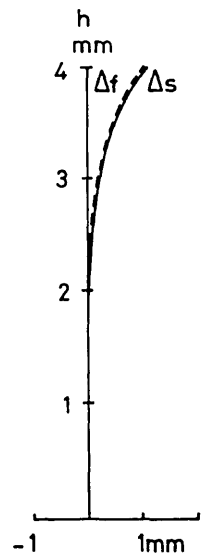

FIG. 14. Spherical aberration of model with lens consisting of seven shells.

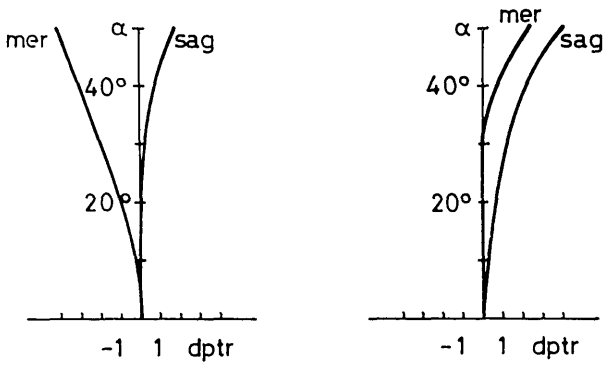

FIG. 15. Astigmatism of emmetropic human eyes according to Ferree and Rand. Classes (a) and (b).

interesting to study the contribution to focusing by the individual refracting surfaces (Fig. 12). The ordinate values in this figure are relative, that is, f_m^1/f_0 for the front surface, and γ_0/γ_i for r_2, r_3, and r_4, with γ_i the convergence ratio, (or angular magnification), whereas f_0, γ_0 are the corresponding values on axis. For a given visual angle

$$f_m = f_0 \cdot (f_m^1/f_0) \cdot (1/\gamma_2) \cdot (1/\gamma_3) \cdot (1/\gamma_4). \qquad (8)$$

Finally, longitudinal meridional comatic aberration along the principal rays, as in Fig. 9 for astigmatism, is shown in Fig. 13 for a series of visual angles.

DISCUSSION

A. Spherical Correction

Figure 5 shows that spherical aberration of the proposed eye model agrees to order of magnitude with experimental findings. On the other hand, the sine condition is not well satisfied, which leads to asymmetry of the coma curves (Fig. 13). It is likely that this shortcoming of the model is due to its neglect of the shell

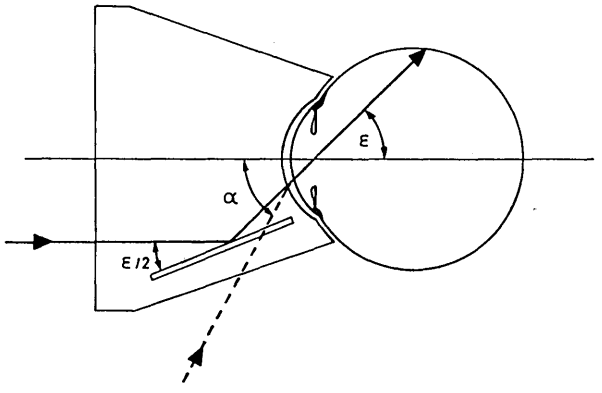

FIG. 16. Eye model with aspherics in combination with plano-concave contact glass (ECG system). For ray tracing, the angle between the principal ray and the mirror was assumed to be $\epsilon/2$, so that incidence on the front surface of the contact glass is at right angles.

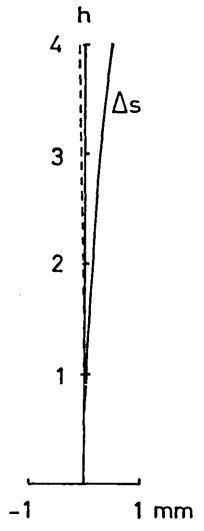

FIG. 17. Spherical aberration of ECG system. Scale of sine-condition aberration is comparable to that of Fig. 5.

structure of the lens. For the rabbit lens, the computations of Nakao *et al.*[10] show that the heavy spherical undercorrection of a fictitious homogeneous lens is reduced to practically zero by the actual shell structure. At the same time, the sine condition is better satisfied.[18] By analogy to his findings, a rough and purely hypothetical shell model for the human lens was constructed, consisting of seven shells, the thicknesses of which decrease and their radii increase with distance from the center, according to square-root laws, with refractive indices varying from 1.38 to 1.41 in steps of 0.005. When this model was substituted for the homogeneous lens of Table I, a similar result was obtained. Spherical aberration and the sine condition of this system are shown in Fig. 14. However, we felt it would be pre-

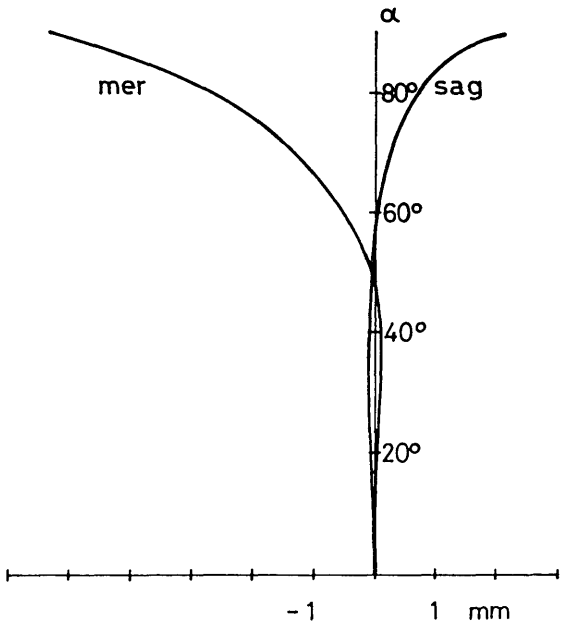

FIG. 18. Astigmatism of ECG system.

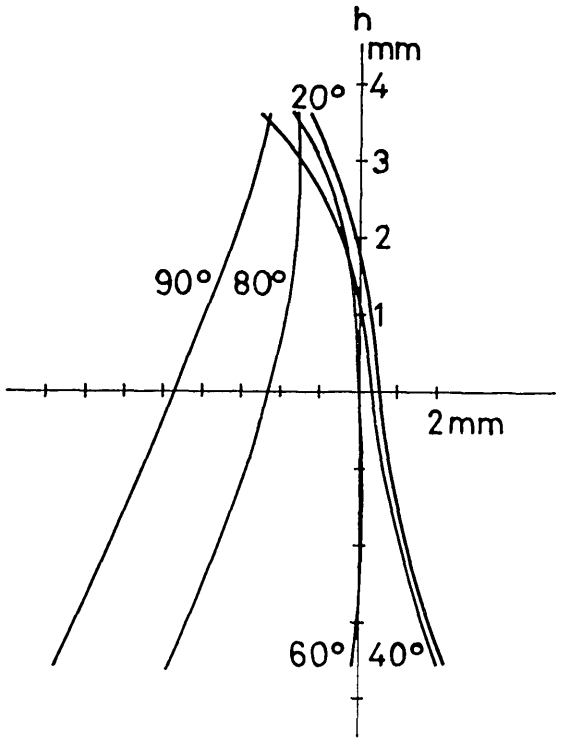

FIG. 19. Longitudinal comatic aberration of ECG system. See remarks to Fig. 13.

mature to do extended ray tracing through this system before more experimental data on the human lens become available.

Furthermore, the advantages of a relatively simple model would be lost.

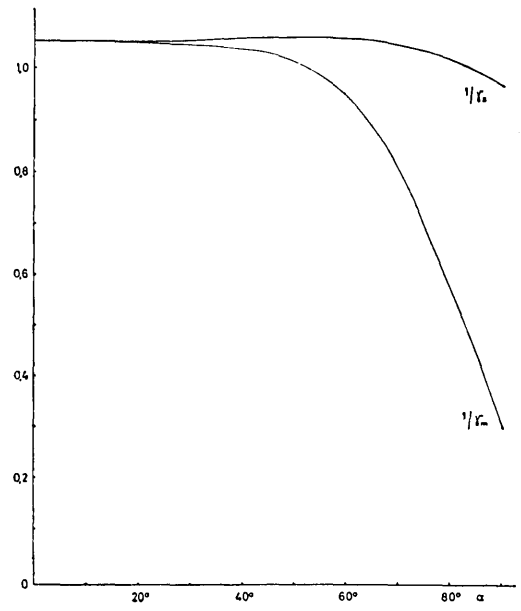

FIG. 20. Meridional and sagittal convergence ratios of ECG system.

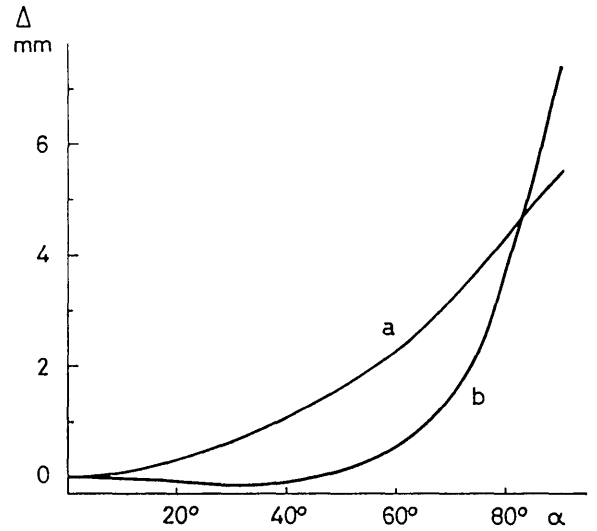

FIG. 21. Sturm's interval, Δ, for eye model with aspherics (a), and ECG system (b).

B. Astigmatism

Figure 9 shows that the location of the retina, up to a visual angle of 90°, is roughly half the distance between the meridional and sagittal foci, i.e., the locus of the circle of least confusion. Strictly speaking this applies only to bundles of infinitesimal numerical aperture, but the coma curves of Fig. 13 indicate that for the present model the circle of least confusion of larger meridional bundles lies not very far from the meridional focus in the stricter sense.

Ferree and Rand[5] concluded from a relatively restricted number of cases that, with respect to astigmatism in the periphery, emmetropic human eyes fall into two distinct classes A and B, which are shown in Fig. 15. Rempt *et al.*,[6] having measured nearly 900 eyes, found however that intermediate cases exist as well. Types A and B of Ferree and Rand may be considered to correspond roughly to the limiting cases. Of 217 emmetropic eyes, 62% were of type A, which therefore is taken to be the "normal type" by Rempt *et al.* From comparison of Figs. 9 and 15, it is evident that the present model comes close to this type. Sturm's interval at 50° visual angle in Fig. 15(a) is 5.5 diopters. The model, for the same visual angle, results in −0.55-mm deviation for the meridional and +1.05 mm for the sagittal focus. When these figures are converted to diopters, taking the respective focal lengths (Fig. 11) into account, we obtain a value of 6.25 diopters for Sturm's interval. In view of the simplifications made in our model, the agreement must be considered good.

For Gullstrand's eye model with spherical surfaces, on the other hand, Sturm's interval at 50° visual angle was found to be 15.1 diopters. Thus, the shape of the cornea has a strong influence on astigmatism in the periphery. Curves like those of class B of Ferree and

Rand might therefore be explained by assuming a shape for the profile curve somewhat more flattened than that corresponding to Eq. (3).

C. Variation of Focal Length with Incidence Angle

From Fig. 12, the decrease of meridional focal length at high visual angle is preponderantly due to the front surface of the lens (r_3), and not to the cornea. This can be understood because ray tracing gives angles of incidence of the principal rays at the lens surface that are larger than at the cornea. The cosines of these angles govern the variation of the convergence ratio.

D. Coma

It is not clear at this time to what extent the calculated curves approximate those of a more refined model that takes the shell structure of the lens into account; nor, owing to lack of experimental data on coma, do we know how they agree with reality.

THE SYSTEM EYE PLUS CONTACT GLASS (ECG)

Rays were traced through the same eye model preceded by a plano-concave plastic lens (Goldmann 3-mirror contact glass,[19] Fig. 16). This lens is characterized by $r_1=\infty$, $r_2=+7.8$ mm, $d=22$ mm, $n_d=1.492$. It is separated from the cornea by 0.2 mm of water ($n_d=1.336$).

As the compound system is nearly afocal ($f=462.4$ mm), we used convergent incident bundles. Their foci were adjusted to a distance behind the first surface such that the circle of least confusion, after passage of the bundles through the system, approximately coincides with the retina. The difference of this distance for bundles of 0° and 80° visual angle was found to be 2 mm.

Spherical, astigmatic, and comatic aberrations are shown in Figs. 17–19, and the dependence of the convergence ratio on visual angle in Fig. 20. Comparison of Figs. 18 and 9 shows that astigmatism is less for the ECG system up to a visual angle of 80° (Fig. 21). This explains the superior image quality provided by use of the Goldmann contact glass. On the other hand, the difference vanishes at the highest visual angles, where the influence of the front surface of the crystalline lens evidently predominates. The steep rise of astigmatism in the case of the ECG system explains also the high efficiency of scleral indentation in regard to image quality.

The coma curves of Fig. 19 undergo a reversal of asymmetry with increasing visual angle. This, too, must be ascribed to the contact glass, because it is not noted in Fig. 13.

Figures 11 and 20 show that in the ECG system the decrease of the meridional convergence ratio is shifted to higher visual angles, reflecting the behavior of astigmatism. This result may be expected to hold also for a model with a more refined lens structure.

ACKNOWLEDGMENTS

Drs. A. Dalcher of Kern & Co., Aarau, and A. Roulier did the programming and ray tracing. The drawings were made by H. R. Däppen.

REFERENCES

*This work has been supported by a grant to the University of Bern, No. NB-03638-05 from the NINDB, National Institutes of Health, Bethesda, Md. 20014.

[1] F. Fankhauser and W. Lotmar, Arch. Ophthalmol. **77**, 320 (1967).

[2] W. Lotmar, F. Fankhauser, and A. Roulier, Arch. Ophthalmol. **82**, 314 (1969).

[3] T. Schmidt, Ophthalmologica **129**, 303 (1955).

[4] F. Fankhauser and J. M. Enoch, Arch. Ophthalmol. **68**, 240 (1962).

[5] C. E. Ferree and G. Rand, in *Report of a Joint Discussion on Vision* (Cambridge U. P., New York, 1932), p. 244.

[6] F. Rempt, J. Hoogerheide, and W. P. H. Hoogenboom, Ophthalmologica **162**, 1 (1971).

[7] F. Fankhauser and W. Lotmar, Acta Ophthalmol. **48**, 253 (1970).

[8] P. Lee, O. Pomerantzeff, and C. L. Schepens, Arch. Ophthalmol. **84**, 650 (1970).

[9] Y. Le Grand, *Optique Physiologique I* (Ed. Rev. Opt., Paris, 1953), p. 52.

[10] S. Nakao, S. Fujimoto, R. Nagata, and K. Iwata, J. Opt. Soc. Am. **58**, 1125 (1968).

[11] G. van den Brink, Vision Res. **2**, 233 (1962).

[12] H. Schober, H. Munker, and F. Zolleis, Opt. Acta **15**, 47 (1968)

[13] F. Berny, Vision Res. **9**, 977 (1969).

[14] R. Bonnet, *La Topographie Cornéenne* (Desroches, Paris, 1964).

[15] R. Bonnet and P. Cochet, Bull. Soc. Franç. Ophtalmol. **73**, 688 (1960).

[16] Visual angle α (Fig. 1) is different from the angle α in Fig. 2 and Eq. (1) as used by Bonnet.

[17] W. Merté, in *Handbuch der Physik XVIII*, edited by H. Geiger and K. Scheel (Springer, Berlin, 1927), p. 73.

[18] S. Nakao, personal communication.

[19] H. Goldmann and T. Schmidt, Ophthalmologica **149**, 481 (1965).